

FULL PAPER

Novel VEGFR-2 inhibitors with an *N*-acylhydrazone scaffold

Fernanda P. Pauli^{1,2} | Juliana R. Martins³ | Thaysa Paschoalin⁴ | Marisa Ionta³ |
 Maria Leticia C. Barbosa^{1,5} | Eliezer J. Barreiro¹ 

¹Laboratory of Evaluation and Synthesis of Bioactive Substances (LASSBio), Institute of Biomedical Sciences, Federal University of Rio de Janeiro, CCS, Rio de Janeiro, RJ, Brazil

²Graduate Program in Chemistry (PGQu), Federal University of Rio de Janeiro, Rio de Janeiro, Brazil

³Department of Drugs and Medicines, Institute of Biomedical Sciences, Federal University of Alfenas, Alfenas, Brazil

⁴Department of Biophysics, Federal University of São Paulo, São Paulo, Brazil

⁵Faculty of Pharmacy, Federal University of Rio de Janeiro, Rio de Janeiro, Brazil

Correspondence

Eliezer J. Barreiro, Institute of Biomedical Sciences, Federal University of Rio de Janeiro, Av Carlos Chagas Filho, 373, Room 203, CCS, UFRJ, Rio de Janeiro 21941-910, Brazil.
 Email: ejbarreiro@ccsdecania.ufrj.br

Abstract

Vascular endothelial growth factor receptor 2 (VEGFR-2) is a tyrosine kinase that mediates a large number of cell responses associated with angiogenesis. The control of the angiogenic pathway in tumorigenesis by the inhibition of VEGFR-2 is considered a promising therapeutic strategy for the prevention and control of solid tumor growth. In this study, the design, synthesis, and biological evaluation of a novel series of VEGFR-2 inhibitors with an *N*-acylhydrazone (NAH) scaffold (**9a–h**) are reported. The molecular design is validated by docking studies and by in vitro inhibitory activity assays. Compounds **9b**, **9c**, **9d**, and **9f** effectively inhibited neo-vascularization induced by VEGF in the chorioallantoic membrane assay. Thus, these NAH derivatives are promising antiangiogenic prototypes.

KEYWORDS

angiogenesis inhibitor, kinase inhibitor, LASSBio-2027, *N*-acylhydrazone, VEGFR-2

1 | INTRODUCTION

Angiogenesis is the formation of new blood vessels from pre-existing ones, representing an important tool for tumor growth and cancer progression.^[1–4] Initially, the tumor cells' energy supply is provided by nearby blood vessels.^[5] However, when the tumor reaches a certain size, the oxygen and nutrient supply is no longer sufficient and new blood vessels are required to ensure tumor progression.^[4,6] The acquisition of an angiogenic phenotype by tumor cells may occur through genetic or tumor environment alterations, leading to the activation of endothelial cells, that is, blood vessel constituent cells.^[7,8] One way of activating endothelial cells is by expression of proangiogenic growth factors, for example, VEGFs (vascular endothelial growth factors), which then activate the corresponding receptors and stimulate angiogenesis.^[5,9,10]

Vascular endothelial growth factor receptor 2 (VEGFR-2) is a tyrosine kinase (TK) that mediates a large number of cell responses associated with angiogenesis.^[11,12] The association of this receptor and the progression of solid tumors are well established in the literature and well validated by experiments.^[13–16] For this reason, modulation of VEGFR-2 has been considered a strategical druggable oncology approach.^[17–21] Moreover, targeting tumor angiogenesis confers relative

selectivity to tumor tissues, which are more sensitive to antiangiogenic effects, and enables targeting a wide range of heterogeneous tumors that share in common an intensified angiogenic signaling.^[22–24]

For these reasons, VEGFR-2 inhibitors, whether combined or not with other therapies, such as chemotherapy and radiotherapy, are employed in the treatment of different types of solid tumors.^[8,9,24–26]

Several VEGFR-2 inhibitors have already been reported in the literature, showing different molecular patterns and distinct pharmacological profiles.^[27,28] The US Food and Drug Administration (FDA) has already approved 48 small molecular entities with kinase inhibitory properties,^[29] among which there are several VEGFR-2 inhibitors, for example sorafenib^[30,31] **1**, sunitinib^[32–35] **2**, axitinib^[36–38] **3**, and cabozantinib^[39,40] **4** (Figure 1).^[41,42]

Vatalanib (**5**; PTK787; Figure 1) is one of the most potent and selective first-generation VEGFR inhibitors, consisting of an aminophthalazine derivative synthesized in 2000 by Novartis.^[43,44] This derivative (**5**) has IC₅₀ values of 110, 43, and 195 nM for VEGFR-1, -2, and -3, respectively.^[45,46] Through theoretical studies of the binding mode of vatalanib (**5**) with VEGFR-2, Manley and colleagues proposed the alteration of the aminophthalazine moiety to the anthranilamide system, creating AAL-993 (**6**; Figures 1–3a).^[47,48] The anthranilamide scaffold of **6** is able to form an intramolecular hydrogen bond involving aniline (NH)

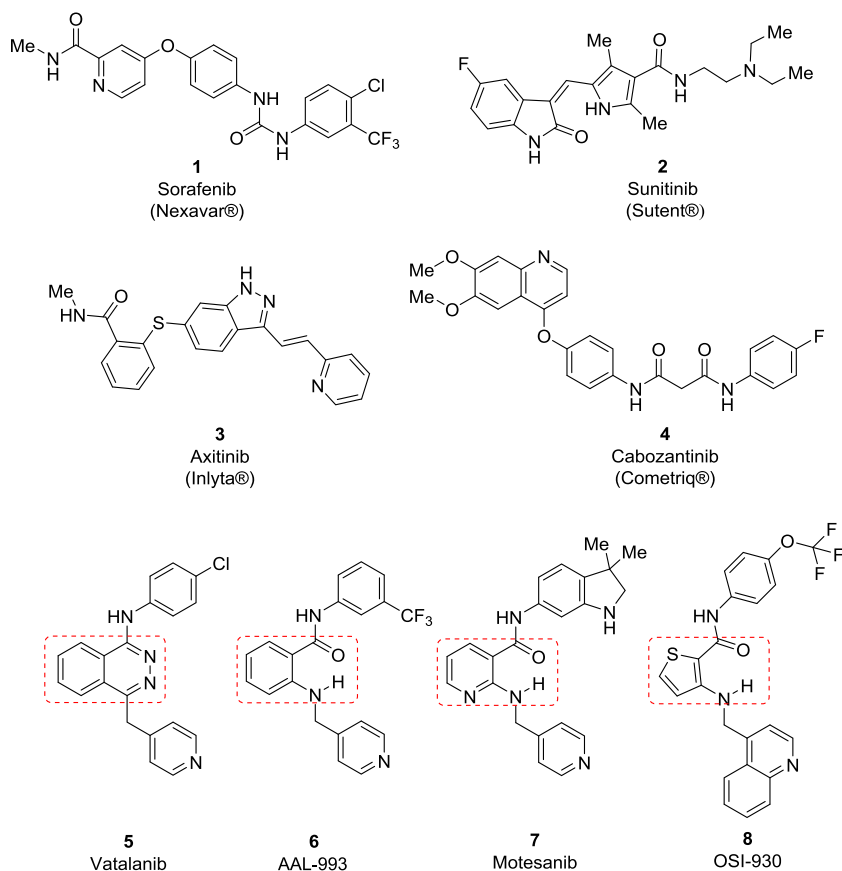


FIGURE 1 VEGFR-2 inhibitors (1–8) previously described in the literature

and benzamide carbonyl (C=O), producing a pseudo-bicyclic mimetic system.^[47,48] In these derivatives, the intramolecular hydrogen bond is stable under biological conditions and promotes a conformational constraint that could mimic the bicyclic system of 5 during ligand–target recognition.^[48–50] Motesanib (7; AMG 706; Figure 1) is also a VEGFR-2 inhibitor^[51,52] (IC₅₀ = 3 nM)^[53] with similar structural characteristics.^[54] Compound OSI-930 (8; Figure 1), bearing a thiophene moiety, is a

VEGFR-2 inhibitor prototype (IC₅₀ = 9 nM),^[55] which is also able to form a similar intramolecular hydrogen bond.^[56,57]

Compound 6 has an IC₅₀ value of 23 nM for VEGFR-2, 130 nM for VEGFR-1, and 18 nM for VEGFR-3, and it also inhibits PDGFR-β with an IC₅₀ value of 640 nM.^[47] In addition, AAL-993 (6) presents in vivo oral bioavailability and proven blockade of VEGF-induced angiogenesis, preventing tumor growth in a range of rodent models.^[58] X-ray crystallography studies have shown that compound 6 is a type II inhibitor, which interacts with VEGFR-2 in DFG-out inactive conformation, as observed in crystallographic complex available in PDB (5EW3; Figure 3a).^[48]

Therefore, considering our continuous research interest in the discovery of new bioactive *N*-acylhydrazone (NAH) derivatives,^[59] we have identified compound 6, bearing an aryl-benzamide moiety, as an attractive molecular scaffold for the design of novel NAH derivatives as VEGFR-2 inhibitor candidates. Herein, we described the in silico design, synthesis, and bioevaluation of a new series of NAH derivatives (9a–h; Figure 2) as VEGFR-2 inhibitors.

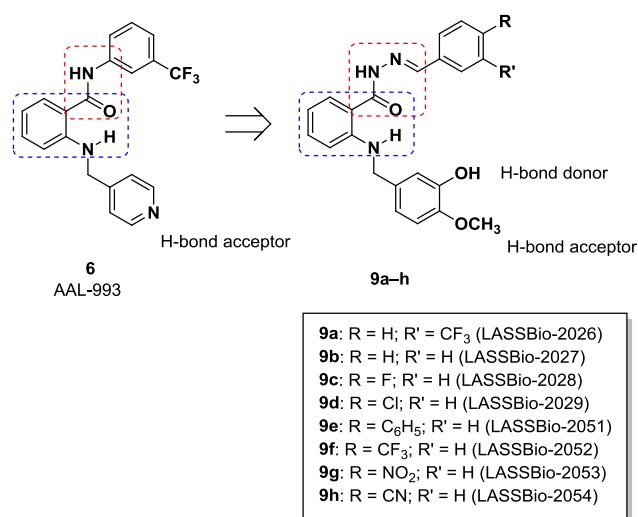


FIGURE 2 The structural design of the novel *N*-acylhydrazone derivatives as VEGFR-2 inhibitors

2 | RESULTS AND DISCUSSION

2.1 | Design of the novel NAH derivatives

The molecular design of the novel NAH derivatives 9a–h (Figure 2) as VEGFR-2 inhibitors was based on the binding mode of ALL-993 (6) with VEGFR-2, which was observed in the crystallographic complex

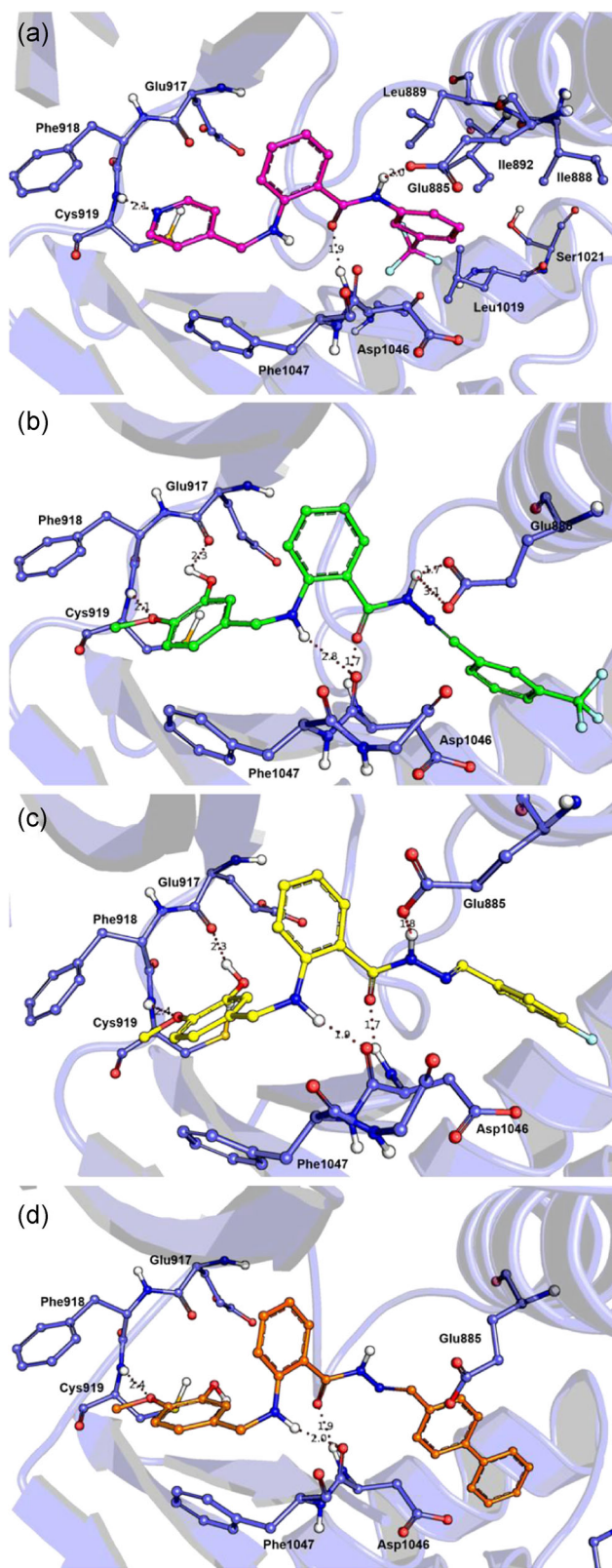


FIGURE 3 (a) The cocrystal structure of AAL-993 in complex with human VEGFR-2 (PDB code: 5EW3); (b) predicted binding interactions of **9a** (green) with VEGFR-2; (c) predicted binding interactions of **9c** (yellow) with VEGFR-2; (d) predicted binding interactions of **9e** (yellow) with VEGFR-2. Docking studies were performed with the GOLD 5.1 program. The images were generated with PyMol software

available in Protein Data Bank with code 5EW3^[58] (Figure 3a). The molecular recognition of **6** by the kinase domain of VEGFR-2 is based primarily on three hydrogen-bond (H-bond) interactions: (a) pyridine N with backbone NH of hinge cysteine (Cys919); (b) anthranilamide-C=O core with backbone NH of DFG aspartate (Asp1046); (c) amide NH of **6** with carboxylate of glutamate side chain (Glu885).^[48] To optimize this interaction mode with VEGFR-2, the first work hypothesis of this study was based on the introduction of a molecular modification in **6** to include additional interaction points in molecular recognition. This approach was envisaged by exploring the glutamate (Glu917) residue placed next to the hinge cysteine (Cys919) of VEGFR-2 ATP-binding site (Figure 3). As Glu917 residue could interact as a hydrogen-bond acceptor, we decided to replace the pyridine ring of **6** by the isovanillin system.^[60,61] The isovanillin scaffold could participate as an H-bond acceptor, similar to the pyridine ring of **6**; also, this oxygenated scaffold has a supplementary H-bond donor at the *meta* position of the phenyl ring, enhancing interactions with Glu917 (Figure 2).

In the novel NAH derivatives (**9a-h**), the anthranilamide moiety of prototype **6** was preserved and the amide linker was replaced by the NAH scaffold.^[59,62] The exchange of the amide spacer of **6** by NAH function in the novel derivatives (**9a-h**) conserves the H-bond donor and acceptor properties,^[59] essential for the recognition of these ligands by the ATP-binding site of VEGFR-2. Finally, substitutions on the phenyl ring adjacent to the NAH imine carbon were also planned on the basis of the sufficient space available in this allosteric binding region.^[63] Initially, derivative **9a** bearing a *meta*-trifluoromethyl group at the original position of **6** was designed. Derivative **9b** was also planned to evaluate the eventual contribution of ring substituents toward the VEGFR-2 inhibitory profile. As the inductive and mesomeric effects primarily depend on the nature of the substituent, different groups were evaluated at the phenyl ring, aiming to explore additional interactions with the hydrophobic pocket adjacent to the DFG of VEGFR-2. The *para*-substitution of the phenyl ring was chosen, as it could potentially present a greater contribution in electronic effects as compared with the *meta* position. The derivative **9f**, bearing the trifluoromethyl substituent at the *para* position ($\sigma = 0.54$) of the phenyl group; the derivatives **9c** (*para*-F, $\sigma = 0.06$) and **9d** (*para*-Cl, $\sigma = 0.23$), with halogenated substituents; **9g** and **9h**, having electron-withdrawing substituents with a distinct σ -value (e.g., *para*-NO₂, $\sigma = 0.78$; *para*-CN, $\sigma = 0.66$); and **9e**, bearing a biphenyl group (*para*-Ph, $\sigma = -0.01$), were designed to evaluate the contribution of potential hydrophobic interactions with the allosteric adjacent binding site of VEGFR-2 (Figure 2).

2.2 | Molecular docking studies

A docking study of this new series of NAH ligands with the TK domain of VEGFR-2 was performed to validate the structural design. According to the results obtained with the semirigid docking approach, the novel NAH derivatives **9a-h** interact with the VEGFR-2 ATP-binding site in a similar conformation as **6** in the reference

TABLE 1 Distances (in Å) for the H-bond interactions between the amino acid residues of VEGFR-2 and the atoms present in the NAH derivatives

Derivatives	Cys919	Glu917	Asp1046 (C=O)	Asp1046 (NH)	Glu885
9a	2.1	2.3	2.8	1.7	1.7
9b	2.1	2.1	2.0	-	2.0
9c	2.4	2.3	1.8	1.7	1.8
9d	2.3	2.3	2.1	1.9	1.9
9e	2.4	-	1.9	2.0	-
9f	2.2	2.1	3.4	2.1	1.9
9g	1.8	2.1	2.0	3.0	1.7
9h	2.6	3.5	2.1	-	-
6	2.1	-	-	1.9	2.0

Note: Only H-bond interactions lower than 3.5 Å lengths were considered.

crystallographic structure (PDB: 5EW3), as shown in Figure 3b,c for compounds 9a and 9c, respectively.

Hydrogen bonds are observed between the isovaniline-OCH₃ and the backbone NH of the Cys919; the isovaniline-OH and the backbone CO of Glu917; and the NH of the NAH group and the side-chain carboxylate of Glu885. Some derivatives also showed interactions involving the carbonyl of the NAH scaffold and the backbone NH of the DFG aspartate residue (Asp1046; Figure 3b,c). Very recently, the binding mode of NAH function with Glu885 and Asp1046 has also been observed by Abdel-Mohsen et al.^[64]

In turn, the biphenyl derivative 9e was not able to form an additional H-bond with Glu917, probably due to steric limitations caused by its larger substituent, as depicted in Figure 3d. Table 1 describes the binding lengths of the H-bond interactions observed

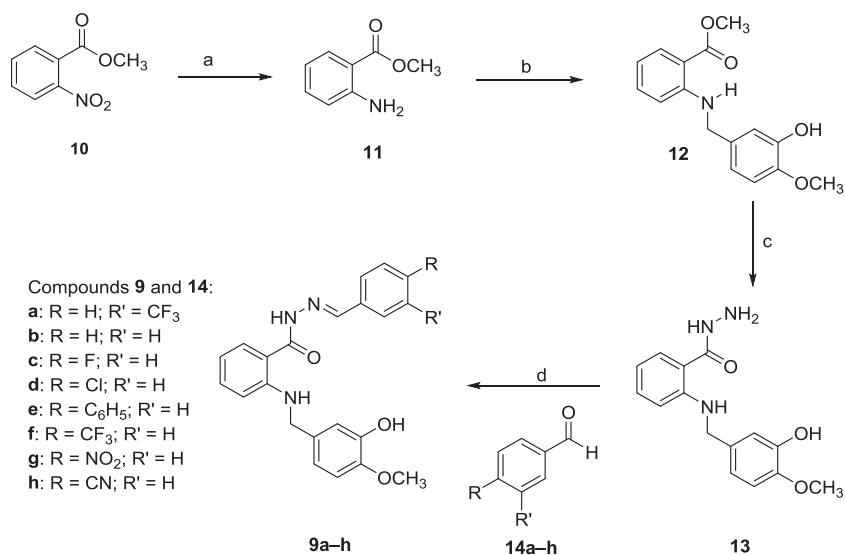
between each NAH compound and the amino acid residues of VEGFR-2.

It is worth mentioning that the results obtained by molecular docking indicate that the replacement of the amide function by the NAH scaffold did not alter the expected bioactive conformation, preserving the pseudo ring with the intramolecular hydrogen bond observed in the prototype 6 for the designed NAH derivatives, except 9h (Figure S34). Moreover, the isovanillin moiety was shown in silico to be able to introduce an additional hydrogen bond with the VEGFR-2 hinge, validating the molecular design of these novel derivatives (9a-h).

2.3 | Chemistry

The synthesis of the novel NAH derivatives 9a-h was realized through the methodology depicted in Scheme 1. In the initial reaction of the synthetic route, methyl 2-nitrobenzoate (10) was reduced to the methyl 2-aminobenzoate (11), using iron and ammonium chloride in a mixture of ethanol/water at reflux.^[12] Next, the benzylaniline derivative 12 was prepared through reductive amination reaction of 11 with 4-methoxy-3-hydroxybenzaldehyde, using sodium cyanoborohydride (NaBH₃CN) and zinc chloride in methanol at room temperature.^[65,66] Then, ester 12 was converted to the respective hydrazide 13 by hydrazinolysis reaction in ethanol under reflux.^[67] Finally, the NAH derivatives 9a-h were synthesized by acid-catalyzed condensation between the key intermediate compound 13 and the respective aldehydes 14a-h.^[66,67]

For all synthesized NAH derivatives, a single NH amide peak at δ 12–11 ppm in ¹H nuclear magnetic resonance (NMR) spectrum (see Supporting Information Data) suggests that only one diastereoisomer of the NAH group was obtained. However, there is strong experimental evidence for the *E*-isomer formation in the condensation step of the NAH's synthetic route.^[62,68]



SCHEME 1 The synthetic route employed for the preparation of the designed *N*-acylhydrazone compounds 9a-h. Reagents and conditions: (a) Fe⁰, NH₄Cl, /H₂O, 80°C, 1hr, 74%; (b) 4-methoxy-3-hydroxybenzaldehyde, ZnCl₂, NaBH₃CN, MeOH, room temperature (r.t.), 48hr, 80%; (c) N₂H₄·H₂O, EtOH, 80°C, 71%; (d) aromatic aldehydes, cat., EtOH, r.t., 4–8hr, 40–85%

2.4 | Biology

2.4.1 | VEGFR-2 inhibition

NAH derivatives **9a–h** were evaluated for their VEGFR-2 inhibitory activity employing the TR-FRET (Cerep-FR[®]) assay at a screening concentration of 1 μ M. From the eight novel chemical entities synthesized in this series, six NAHs have demonstrated a percentage of inhibition >85%, highlighting **9b**, **9c**, and **9h** derivatives, which induced 98% inhibition (Figure S35) in the screening assay. In turn, derivatives **9e** and **9f** did not reach 50% inhibition at this concentration. For compound **9e**, the bulky biphenyl residue prevents its accommodation at the ATP-binding site, which could explain the poor activity. In turn, for derivative **9f**, although the docking study has indicated a favorable

interaction with the VEGFR-2 hinge region, this ligand–target recognition was not culminating in a potent inhibition of the kinase activity in vitro. However, in general, the results obtained in the VEGFR-2 inhibition assay are in accordance with those obtained in the docking study, suggesting that the designed NAH derivatives are favorable for the development of VEGFR-2 inhibitors with a novel chemical scaffold.

2.4.2 | Antiangiogenic activity

Considering the key role of VEGFR-2 signaling in angiogenesis, the novel series of NAH derivatives was assayed to evaluate its antiangiogenic activity through chick embryo chorioallantoic membrane (CAM) assay.

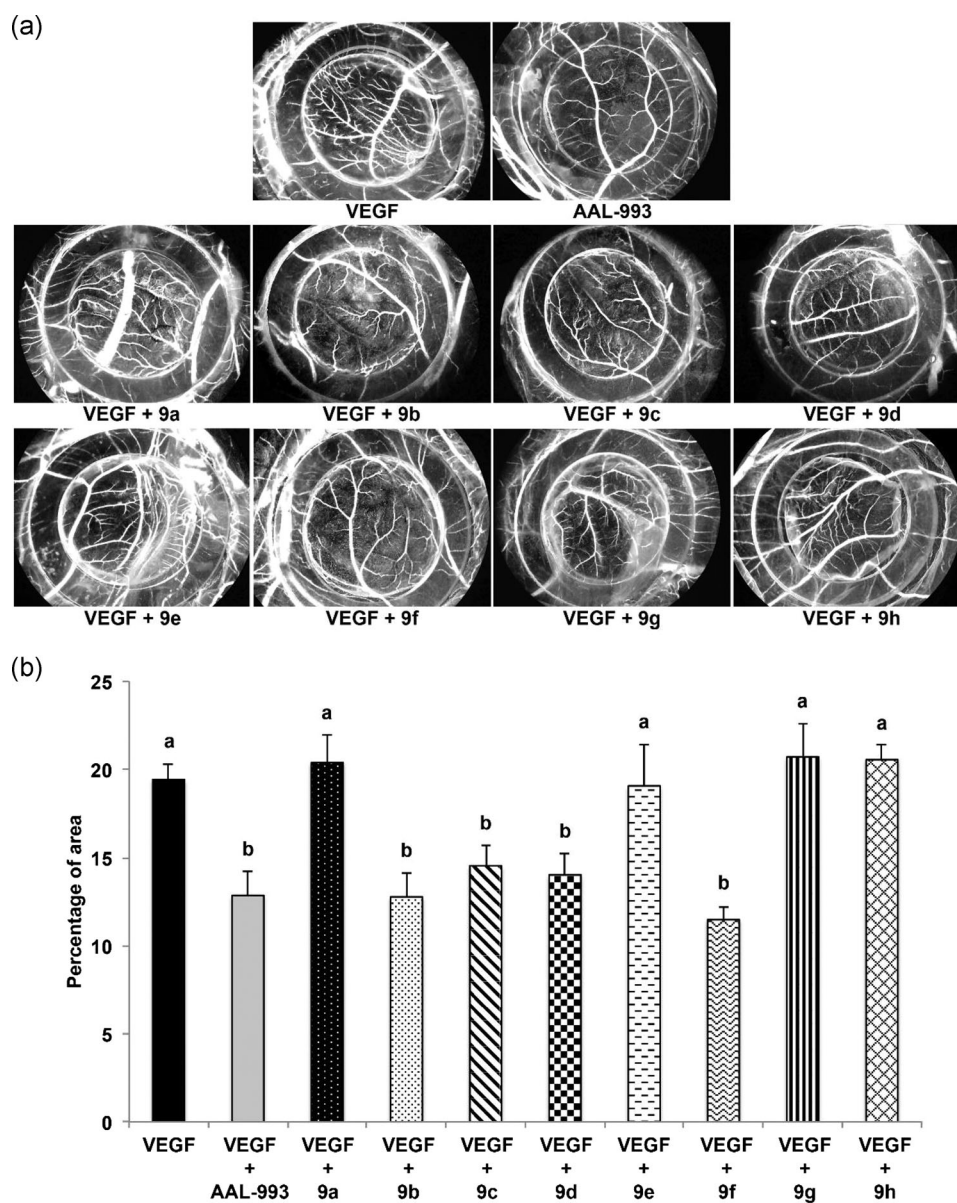


FIGURE 4 (a) Illustrative images obtained from chorioallantoic membrane (CAM) assays using a stereomicroscope (magnification, $\times 2$). (b) The quantitative analysis of the CAM assays. Different letters indicate significant differences ($p < .05$) according to analysis of variance with post-hoc comparisons by the Holm–Sidak multiple comparison test

CAM is an extraembryonic membrane formed on Days 3–4 of chicken development by the fusion of the chorion and the allantois that contain a blood vessel network. Between Days 8 and 10, the developing CAM vasculature is ready to sprout in response to additional proangiogenic stimuli, which, in turn, is very responsive to antiangiogenic factors.^[69] Thus, NAH derivatives **9a–h** or AAL-993 (**6**) were inoculated on CAM in the presence of VEGF in chicken embryos with 8 days of development, and the area of the blood vessels was evaluated on the 10th day.

The amount of NAH derivatives used in CAM assays was defined from the dose–response curve using the substance LASSBio-2027 (**9b**) at 0.1, 1, and 10 ng/CAM for 48 hr. Reduction in blood vessels area was observed only in samples treated with 0.1 and 1 ng/CAM combined with VEGF as compared with the VEGF group (Figure S44). Thus, further CAM assays were carried out using 1 ng/CAM (equivalent to 0.1 $\mu\text{mol/l}$) of NAH derivatives. There was no cytotoxic effect of these substances on human umbilical vein endothelial cells (HUVECs) when they were used at 0.1 $\mu\text{mol/l}$ for 48 hr (data not shown). The amount of proangiogenic (VEGF) and antiangiogenic (AAL-993) agents used in CAM assays was defined from cell viability assay using HUVEC cells (Figure S45).

Among the eight substances tested, **9b**, **9c**, **9d**, and **9f** effectively inhibited neovascularization induced by VEGF (Figure 4) in the CAM assay. These substances apparently reduced the formation of new blood vessels induced by VEGF. We observed a lower percentage of vessel area in samples treated with **9b**, **9c**, **9d**, or **9f** combined with

VEGF as compared with the group treated only with VEGF where sprouting of microvessels was widely observed. The antiangiogenic activity of **9b**, **9c**, **9d**, and **9f** was equivalent to that observed for AAL-993 (Figure 4). There were no significant differences in samples treated with **9a**, **9e**, **9g**, or **9h** combined with VEGF in comparison with the VEGF group (Figure 4) in tested experimental conditions. These findings showed some inconsistencies regarding results obtained from biochemical assay. For example, **9a**, **9g**, and **9h** were unable to inhibit neovascularization in the CAM assay, but they inhibited VEGFR-2 activity in the biochemical assay. Discrepancies between the enzymatic assay and cell-based models are not uncommon^[70,71] and may be related to the high complexity of the in vivo model, compared with biochemical assays where purified kinase domain of VEGFR-2 is used.

In the next step, we performed an additional assay to evaluate a better antiangiogenic activity of the substance **9f**. For this tube formation assay using HUVECs with compounds **9e** and **9f**, which displayed negative and positive effect on neovascularization in CAM assay, respectively. We observed a dense and regular network with long wide branches in HUVEC control cultures. A similar pattern was observed in cultures treated with **9e**, indicating that VEGF induced the formation of capillary-like structures in these samples. By contrast, we observed a broken network and dispersed cell clusters in cultures treated with **9f**, demonstrating that this substance effectively interfered in capillary-like tube formation of HUVECs on the Matrigel surface (Figure 5). Thus, we demonstrated that **9f**

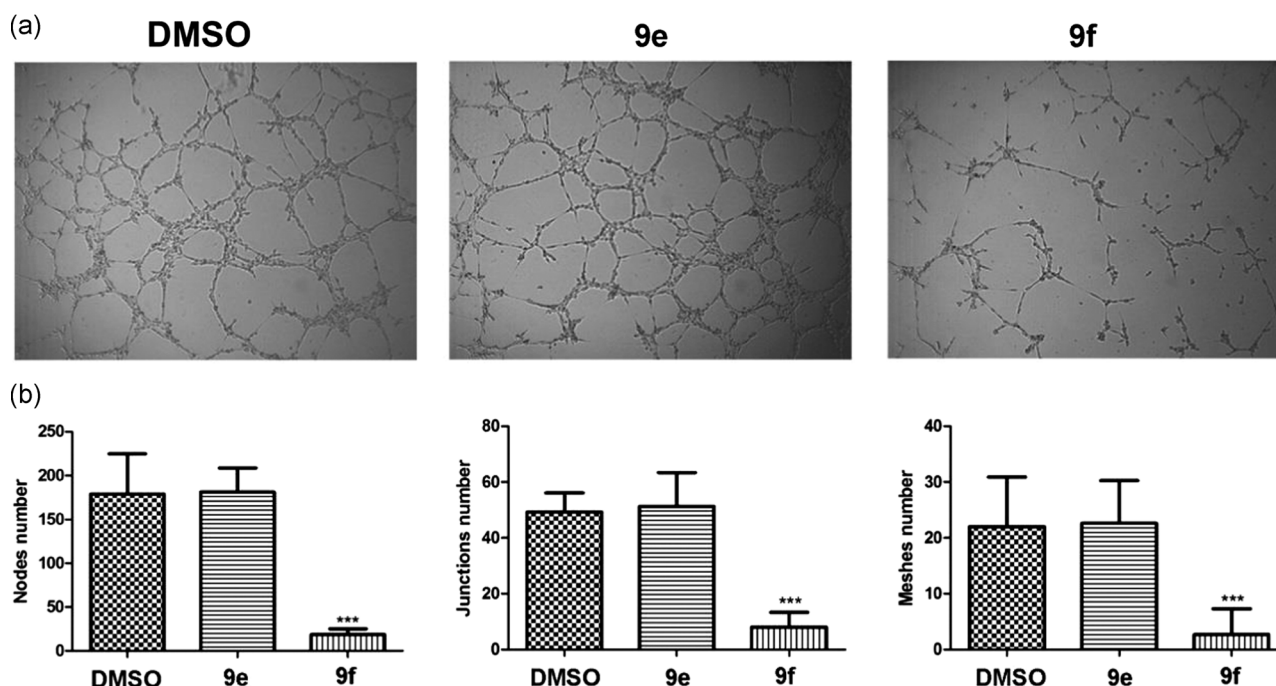


FIGURE 5 (a) Illustrative images of the tube formation assays ($\times 10$ magnification). HUVECs were plated on Matrigel and treated for 18 hr with substances **9e** or **9f** at 0.1 $\mu\text{mol/l}$. (b) The tube formation assay analysis: The ability of HUVECs to form capillary-like structures was evaluated considering the number of nodes, junctions, and meshes formed. These parameters were determined using Angiogenesis Analyzer from ImageJ Program. *** $p < .001$ according to analysis of variance, followed by Dunnett's post-test. DMSO, dimethyl sulfoxide; HUVEC, human umbilical vein endothelial cell

effectively acted on endothelial cells, inhibiting cell proliferation and migration, thereby acting as an antiangiogenic agent.

In the last few decades, many efforts have been made to identify new angiogenesis inhibitors^[72] due to tumor resistance and toxicity associated with the use of currently available antiangiogenic treatment.^[73] Our findings revealed that **9b**, **9c**, **9d**, and **9f** are promising prototype derivatives for antiangiogenic therapy once they effectively reduce the neovascularization induced by VEGF. Curiously, antiangiogenic effect was observed when very low doses of these substances were used. It has been reported that low doses of antiangiogenic agents may contribute to tumor vessel normalization and reduction of tumor growth and metastasis.^[74] Further studies should be carried out to evaluate the clinical applicability of these NAH derivatives.

3 | CONCLUSION

In conclusion, in this study, we have described the molecular design, the synthesis, and biological evaluation of a novel series of NAH derivatives (**9a–h**), as $-N=CH-$ homologs of compound **6** and VEGFR-2 inhibitors. The performed docking studies have shown that the designed NAH compounds could potentially form an additional hydrogen bond with the glutamate residue of VEGFR-2 ATP-binding site, validating the molecular design. Furthermore, the enzymatic inhibitory assay and the antiangiogenic activity have shown that the novel NAH derivatives represent a new chemical scaffold for VEGFR-2 inhibitors. Compounds **9b**, **9c**, **9d**, and **9f** effectively inhibited neovascularization induced by VEGF in the CAM assay, highlighting **9f** that showed an equivalent antiangiogenic activity as that observed for the prototype AAL-993.

4 | EXPERIMENTAL

4.1 | Chemistry

4.1.1 | General

Commercial reagents were obtained from commercial suppliers and were used without pretreatment. The reactions were monitored by thin-layer chromatography on silica gel (chromate aluminum sheets Kieselgel 60 F245; Merck), and the visualization of the CCD plates was performed with ultraviolet (UV) light at wavelengths of 254 and 365 nm. For the ^1H and ^{13}C NMR spectra, the samples were dissolved in dimethyl sulfoxide (DMSO)- d_6 and placed in a 5-mm diameter tube. The NMR spectra were obtained in a Bruker DPX-200 (200 and 50 MHz), DRX-300 (300 and 75 MHz), Varian 400-MR (400 and 100 MHz), and 500MR (500 and 125 MHz) spectrometer. The chemical shifts (δ) are reported in parts per million (ppm) from the internal standard tetramethylsilane, and the coupling constant values (J) are given in Hertz (Hz; Figures S1–S16). The areas of the peaks were obtained by electronic integration, and their multiplicities are described as follows: s, singlet; d, doublet; dd, double doublet; ddd,

double double doublet; t, triplet; m, multiplet, sl, single long. For some of the novel NAH derivatives, solubility limitations hampered the clear observation and attribution of the carbonyl carbon in ^{13}C NMR spectra. However, structures were properly elucidated through ^1H NMR and electrospray ionization–mass spectra (ESI–MS), and the presence of the NAH carbonyl was confirmed by infrared (IR) spectra (ν , 1,633–1,639 cm^{-1}) for all NAH derivatives. IR spectra were obtained on an IR Thermo Scientific Nicolet iS10 Smart FT-IR spectrometer, and the absorption values were recorded in wavenumber using the reciprocal centimeter (cm^{-1}) as the unit (Figures S17–S24). High-performance liquid chromatography with photodiode array detection (HPLC–PDA) was performed in Shimadzu-LC20AD apparatus, using the Kromasil 100-5C18 (4.6 \times 250 mm) column, SPD-M20A detector (diode array) at wavelengths of 294–338 nm for analyte quantification and constant flow of 1 ml/min (Figures S25–S32). The mobile phase used was 60% acetonitrile and 40% water. The solvents used for analysis by HPLC–PDA have HPLC purity (TediaBrazil[®]). The melting points (mp.) of all compounds were determined on a Quimis model Q340.23. The molecular ions of the compounds were detected using the Esquire 6000-ESI Ion Trap MSn System Bruker Daltonics mass spectrometer in positive mode.

The InChI codes of the investigated compounds are provided as Supporting Information Data.

4.1.2 | The synthesis of methyl 2-aminobenzoate intermediate (**11**)

In a 50-ml flask, methyl 2-nitrobenzoate (**10**; 43.2 g, 11 mmol) was added in an EtOH/ H_2O (12:6 ml) mixture, along with 5 equivalents of iron (3.0 g; mmol) and 1.6 equivalents of ammonium chloride (0.94 g, 17.60 mmol). The reaction mixture was maintained under reflux at 80°C and was constantly stirred for 1 hr. Then, the reaction mixture was filtered hot through Celite, and the isolation was carried out with separation funnel extraction, using ethyl acetate and water at pH 9 (adjusted with 10% NaOH solution). The organic phase was dried over sodium sulfate, filtered, and the solvent was evaporated under reduced pressure. The final product **11** is a colorless oil obtained in 74% yield. ^1H MNR (400 MHz, DMSO- d_6) δ (ppm): 3.78 (s, 3H, OCH_3), 6.5 (ddd, 1H, $J = 1 \text{ Hz}, 7 \text{ Hz}, \text{ and } 8 \text{ Hz}, \text{ H}_2$), 6.64 (s, 2H, NH_2), 6.76 (dd, 1H, $J = 8 \text{ Hz}, 7 \text{ Hz}, \text{ H}_4$), 7.24 (t, 1H, $J = 8 \text{ Hz}, 7 \text{ Hz}, 2 \text{ Hz}, \text{ H}_3$), 7.68 (dd, 1H, $J = 8 \text{ Hz}, 2 \text{ Hz}, \text{ H}_1$). IR (attenuated total reflection [ATR] cm^{-1}): 3,479, 3,370, 1,687.

4.1.3 | The synthesis of methyl 2-[(3-hydroxy-4-methoxybenzyl)amino]benzoate (**12**)

In a 50-ml flask, methyl 2-aminobenzoate (**11**; 0.86 ml, 6.60 mmol) was added with 1 equivalent of 3-hydroxy-4-methoxybenzaldehyde (41.0 g, 6.60 mmol) and 0.5 equivalent of zinc chloride (ZnCl_2 , 0.45 g, 3.30 mmol). The reaction mixture was stirred at room temperature. After 24 hr, 1 equivalent of sodium cyanoborohydride (NaBH_3CN ,

0.41 g, 6.60 mmol) was added in three portions every half hour. The reaction was terminated after 24 hr of the addition of the reducing agent NaBH_3CN . For isolation, the reaction mixture was kept in an ice bath, and then the precipitate formed was filtered and washed with distilled water. The product is a light gray solid, obtained in 80% yield; mp. 87–89°C. ^1H NMR (400 MHz, $\text{DMSO}-d_6$) δ (ppm): 3.78 (s, 3H, H8), 3.79 (s, 3H, H7), 4.29 (d, 2H, $J = 5$ Hz, CH_2), 6.57 (dd, $J = 8$ Hz, 1 Hz, H2), 6.69–6.76 (m, H1', H3', and H4), 6.87 (d, $J = 8$ Hz, H4'), 7.33 (ddd, $J = 1$ Hz, 8 Hz, 7 Hz, 2 Hz, H3), 7.80 (dd, $J = 8$ Hz, 2 Hz, H1), 7.99 (t, $J = 5$ Hz, NH). ^{13}C NMR (100 MHz, $\text{DMSO}-d_6$) δ (ppm): 45.59 (CH_2), 51.54 (C7), 5.68 (C8), 109.28 (C6), 111.95 (C4'), 112.40 (C2), 114.44 (C4), 114.45 (C1'), 117.79 (C3'), 131.59 (C2'), 134.68 (C3), 146.65 (C6'), 146.74 (C5'), 150.45 (C5), 168.19 ($\text{C}=\text{O}$). IR (ATR, cm^{-1}): 3,502, 3,360, 1,685.

4.1.4 | The synthesis of 2-[(3-hydroxy-4-methoxybenzyl)amino]benzohydrazide (13)

In a 50-ml flask, intermediate **12** (1 g, 3.48 mmol) was added in 10 ml of ethanol and 20 equivalents of 80% hydrazide hydrate (3.39 ml, 69.60 mmol). The reaction mixture was maintained under reflux at 80°C and was stirred. After 12 hr, the reaction was finished and the solvent was evaporated under reduced pressure. The precipitate formed was washed with distilled water to give a light brown solid product in 71% yield; mp. 171–172°C. ^1H NMR (400 MHz, $\text{DMSO}-d_6$) δ (ppm): 3.73 (s, 3H, OCH_3), 4.19 (d, 2H, $J = 5$ Hz, CH_2), 4.41 (s, 2H, NH_2), 6.52 (t, 1H, $J = 7$ Hz, 2H), 6.62 (d, 1H, $J = 8$ Hz, H4), 6.70–6.77 (m, 2H, H1', H3'), 6.86 (d, 1H, $J = 8$ Hz, H4'), 7.20 (t, 1H, $J = 8$ Hz, H3), 7.47 (d, 1H, $J = 8$ Hz, H1), 7.96 (t, 1H, $J = 5$ Hz, NH), 8.94 (s, 1H, OH), 9.58 (s, 1H, NH). ^{13}C NMR (100 MHz, $\text{DMSO}-d_6$) δ (ppm): 45.84 (CH_2), 55.70 (C8), 111.36 (C4'), 112.37 (C2), 114.11 (C6), 114.37 (C4), 114.55 (C1'), 117.38 (C3'), 127.79 (C1), 131.98 (C2'), 132.05 (C3), 146.59 (C6'), 146.65 (C5'), 148.77 (C5), 168.63 ($\text{C}=\text{O}$). IR (ATR, cm^{-1}): 3,393, 3,315, 3,272, 1,633.

4.1.5 | General procedure for the synthesis of the NAH derivatives

The intermediate **13** (0.30 g, 1.0 mmol) was added to a 20-ml flask with 15 ml of ethanol and 1 equivalent of the respective aldehyde (1.0 mmol) and one drop of 37% HCl as a catalyst. The reaction mixture was stirred at room temperature for 4–8 hr until precipitation was observed. For insulation, the solvent was then partially concentrated at reduced pressure and the flask was placed in an ice bath. The precipitate was filtered and dried under vacuum to obtain the NAH derivatives. When necessary, purification was performed, as described in the specifications of the following items.

N'-[3-(Trifluoromethyl)benzylidene]-2-[(3-hydroxy-4-methoxybenzyl)amino]benzohydrazide (9a)

Derivative **9a** was obtained by condensation of intermediate **13** with 1 equivalent of aldehyde **14a** (0.14 ml, 1.0 mmol) in 65% yield. **9a** was

purified by recrystallization with ethanol to give a pale-yellow solid; mp. 172–173°C; purity (HPLC; Figure S25): 99.1%. ^1H NMR (400 MHz, $\text{DMSO}-d_6$) δ (ppm; Figure S1): 3.73 (s, 3H, OCH_3), 4.24 (d, 2H, $J = 5$ Hz, CH_2), 6.63 (t, 1H, $J = 7$ Hz, 2H), 6.69 (d, 1H, $J = 8$ Hz, H4), 6.74–6.79 (m, 2H, H1', H3'), 6.87 (d, 1H, $J = 8$ Hz, H4'), 7.29 (t, 1H, $J = 7$ Hz, H3), 7.64–7.71 (m, 2H, H1'', H2''), 7.78 (d, 1H, $J = 8$ Hz, H1), 7.88 (s, 1H, ArNH), 8.00 (d, 1H, $J = 7$ Hz, H6''), 8.05 (s, 1H, H3''), 8.48 (s, 1H, $\text{N}=\text{CH}$), 8.96 (s, 1H, OH), 11.91 (s, 1H, $\text{O}=\text{CNH}$). ^{13}C NMR (100 MHz, $\text{DMSO}-d_6$) δ (ppm; Figure S2): 45.80 (CH_2), 55.67 (C8), 111.72 (C4'), 112.38 (C2), 113.63 (C6), 114.36 (C4), 114.56 (C1'), 117.88 (C3'), 122.81 (C4''), 125.13 (CF_3), 126.13 (C6''), 128.70 (C1), 128.70 (C1), 129.78 (C1''), 130.05 (C5''), 131.02 (C2''), 131.80 (C3), 133.01 (C2'), 135.69 (C3''), 145.18 ($\text{C}=\text{N}$), 146.63 (C6'), 146.70 (C5), 149.42 (C5'). IR (ATR, cm^{-1} ; Figure S17): 3,213, 3,051, 1,633. ESI-MS (Figure S33) calculated for $\text{C}_{23}\text{H}_{20}\text{N}_3\text{O}_3\text{F}_3$: $[\text{M}]^+ = 443.14$. Found: $[\text{M}+\text{H}]^+ = 444.04$.

N'-Benzylidene-2-[(3-hydroxy-4-methoxybenzyl)amino]benzohydrazide (9b)

Derivative **9b** was obtained by condensation of intermediate **13** with 1 equivalent of aldehyde **14b** (0.10 ml, 1.0 mmol) in 78% yield. The **9b** is a pale-yellow solid; mp. 200–201°C; purity (HPLC; Figure S26): 97.7%. ^1H NMR (400 MHz, $\text{DMSO}-d_6$) δ (ppm; Figure S3): 3.73 (s, 3H, OCH_3), 4.24 (d, 2H, $J = 5$ Hz, CH_2), 6.62 (t, 1H, $J = 7$ Hz, 2H), 6.68 (d, 1H, $J = 8$ Hz, H4), 6.73–6.79 (m, 2H, H1', H3'), 6.87 (d, 1H, $J = 8$ Hz, H4'), 7.28 (t, 1H, $J = 7$ Hz, H3), 7.43–7.48 (m, 3H, H1'', H2'', H6''), 7.63 (d, 1H, $J = 8$ Hz, H1), 7.70 (d, 2H, $J = 8$ Hz, H2'', H4''), 7.87 (s, 1H, ArNH), 8.40 (s, 1H, $\text{N}=\text{CH}$), 8.97 (s, 1H, OH), 11.72 (s, 1H, $\text{O}=\text{CNH}$). ^{13}C NMR (100 MHz, $\text{DMSO}-d_6$) δ (ppm; Figure S4): 45.81 (CH_2), 55.68 (C8), 111.67 (C4'), 112.38 (C2), 113.95 (C6), 114.37 (C4), 114.53 (C1'), 117.87 (C3'), 126.29 (C6''), 128.57 (C1), 128.88 (C1''), C5''), 129.95 (C2'', C4''), 131.86 (C3), 132.82 (C2'), 134.48 (C3''), 146.64 ($\text{C}=\text{N}$), 146.70 (C6'), 147.11 (C5), 149.34 (C5'). IR (ATR, cm^{-1} ; Figure S18): 3,349, 3,279, 2,840, 1,638. ESI-MS (Figure S34): calculated for $\text{C}_{22}\text{H}_{21}\text{N}_3\text{O}_3$: $[\text{M}]^+ = 375.16$. Found: $[\text{M}+\text{H}]^+ = 376.09$.

N'-(4-Fluorobenzylidene)-2-[(3-hydroxy-4-methoxybenzyl)amino]benzohydrazide (9c)

Derivative **9c** was obtained by condensation of intermediate **13** with 1 equivalent of aldehyde **14c** (0.11 ml, 1.0 mmol) in 69% yield. **9c** is a white solid; mp. 176–177°C; purity (HPLC; Figure S27): 99.2%. ^1H NMR (400 MHz, $\text{DMSO}-d_6$) δ (ppm; Figure S5): 3.73 (s, 3H, OCH_3), 4.24 (d, 2H, $J = 5$ Hz, CH_2), 6.62 (t, 1H, $J = 7$ Hz, 2H), 6.68 (d, 1H, $J = 8$ Hz, H4), 6.73–6.79 (m, 2H, H1', H3'), 6.87 (d, 1H, $J = 8$ Hz, H4'), 7.28 (t, 1H, $J = 7$ Hz, H3), 7.43–7.48 (m, 3H, H1'', H2'', H6''), 7.63 (d, 1H, $J = 8$ Hz, H1), 7.70 (d, 2H, $J = 8$ Hz, H2'', H4''), 7.87 (s, 1H, ArNH), 8.40 (s, 1H, $\text{N}=\text{CH}$), 8.97 (s, 1H, OH), 11.72 (s, 1H, $\text{O}=\text{CNH}$). ^{13}C NMR (100 MHz, $\text{DMSO}-d_6$) δ (ppm; Figure S6): 45.79 (CH_2), 55.69 (C8), 111.64 (C4'), 112.64 (C2), 113.93 (C6), 114.34 (C4), 114.53 (C1'), 115.75 (C1'', C5''), 117.85 (C3'), 128.59 (C1), 129.14 (C2'', C4''), 131.09 (C3''), 131.85 (C3), 132.79 (C2'), 145.94 ($\text{C}=\text{N}$), 146.63 (C6'), 146.68 (C5), 149.31 (C5'), 163.01 (d, $J = 249$ Hz, C6''), 165.62 ($\text{C}=\text{O}$). IR (ATR, cm^{-1} ; Figure S19): 3,297, 3,145, 1,633. ESI-MS (Figure S35): calculated for $\text{C}_{22}\text{H}_{20}\text{N}_3\text{O}_3\text{F}$: $[\text{M}]^+ = 393.08$. Found: $[\text{M}+\text{H}]^+ = 394.08$.

N'-(4-Chlorobenzylidene)-2-[[3-hydroxy-4-methoxybenzyl)amino]-benzohydrazide (**9d**)

Derivative **9d** was obtained by condensation of intermediate **13** with 1 equivalent of aldehyde **14d** (0.14 g, 1.0 mmol) in 68% yield. **9d** is a white solid; mp. 168–169°C; purity (HPLC; Figure S28): 98.9%. ¹H NMR (400 MHz, DMSO-*d*₆) δ (ppm; Figure S7): 3.73 (s, 3H, OCH₃), 4.24 (d, 2H, *J* = 5 Hz, CH₂), 6.62 (t, 1H, *J* = 7 Hz, 2H), 6.68 (d, 1H, *J* = 8 Hz, H₄), 6.73–6.79 (m, 2H, H₁', H₃'), 6.87 (d, 1H, *J* = 8 Hz, H₄'), 7.28 (t, 1H, *J* = 7 Hz, H₃), 7.52 (d, 2H, *J* = 9 Hz, H₁'', H₅''), 7.63 (d, 1H, *J* = 8 Hz, H₁), 7.73 (d, 2H, *J* = 9 Hz, H₂'', H₄''), 7.86 (s, 1H, ArNH), 8.38 (s, 1H, N=CH), 8.96 (s, 1H, OH), 11.77 (s, 1H, O=CNH). ¹³C NMR (100 MHz, DMSO-*d*₆) δ (ppm; Figure S8): 45.78 (CH₂), 55.72 (C8), 111.68 (C₄'), 112.37 (C2), 113.80 (C6), 114.35 (C4), 114.51 (C₁'), 117.88 (C₃'), 128.59 (C₁' and C₅''), 128.93 (C₁, C₂' and C₄''), 131.83 (C3), 132.88 (C₂'), 133.43 (C₆''), 134.34 (C₃''), 145.72 (C=N), 146.63 (C₆'), 146.68 (C5), 149.35 (C₅'). IR (ATR, cm⁻¹; Figure S20): 3,403, 3,213, 3,048, 1,638. ESI-MS (Figure S36): calculated for C₂₂H₂₀N₃O₃Cl: [M]⁺ = 409.12. Found: [M+H]⁺ = 410.06.

N'-[[1,1'-Biphenyl]-4-methylene]-2-[[3-hydroxy-4-methoxybenzyl)amino]benzohydrazide (**9e**)

Derivative **9e** was obtained by condensation of intermediate **13** with 1 equivalent of aldehyde **13e** (0.18 g, 1.0 mmol) in 85% yield. **9e** is a light-yellow solid; mp. 204–205°C; purity (HPLC; Figure S29): 99.3%. ¹H NMR (400 MHz, DMSO-*d*₆) δ (ppm; Figure S9): 3.74 (s, 3H, OCH₃), 4.25 (d, 2H, *J* = 5 Hz, CH₂), 6.63 (t, 1H, *J* = 7 Hz, 2H), 6.69 (d, 1H, *J* = 8 Hz, H₄), 6.74–6.80 (m, 2H, H₁', H₃'), 6.87 (d, 1H, *J* = 8 Hz, H₄'), 7.29 (t, 1H, *J* = 7 Hz, H₃), 7.39 (t, 1H, *J* = 7 Hz, H₆''), 7.49 (t, 2H, *J* = 7 Hz, H₁'', H₅''), 7.66 (d, 1H, *J* = 8 Hz, H₁), 7.72–7.82 (m, 6H, H₁'', H₂'', H₄'', H₅'', H₂'', H₄''), 7.90 (s, 1H, ArNH), 8.44 (s, 1H, N=CH), 8.97 (s, 1H, OH), 11.75 (s, 1H, O=CNH). ¹³C NMR (100 MHz, DMSO-*d*₆) δ (ppm; Figure S10): 45.80 (CH₂), 55.72 (C8), 111.65 (C₄'), 112.39 (C2), 113.92 (C6), 114.36 (C4), 114.52 (C₁'), 117.82 (C₃'), 126.65 (C₂' and C₄''), 127.04 (C₁' and C₅''), 127.58 (C₁' and C₅''), 127.86 (C₆''), 128.58 (C₁), 129.02 (C₂' and C₄''), 131.85 (C3), 132.81 (C₂'), 133.59 (C₃''), 139.33 (C₆''), 141.31 (C=N), 146.63 (C₆'), 146.69 (C5), 149.34 (C₅'). IR (ATR, cm⁻¹; Figure S21): 3,408, 3,224, 3,054, 1,639. ESI-MS (Figure S37): calculated for C₂₈H₂₅N₃O₃: [M]⁺ = 451.19. Found: [M+H]⁺ = 452.17.

N'-[4-(Trifluoromethyl)benzylidene]-2-[[3-hydroxy-4-methoxybenzyl)amino]benzohydrazide (**9f**)

Derivative **9f** was obtained by condensation of intermediate **13** with 1 equivalent of aldehyde **14f** (0.14 ml, 1.0 mmol) in 63% yield. **9f** is a light-yellow solid; mp. 172–173°C; purity (HPLC; Figure S30): 99.1%. ¹H NMR (400 MHz, DMSO-*d*₆) δ (ppm; Figure S11): 3.73 (s, 3H, OCH₃), 4.24 (d, 2H, *J* = 5 Hz, CH₂), 6.63 (t, 1H, *J* = 7 Hz, 2H), 6.69 (d, 1H, *J* = 8 Hz, H₄), 6.73–6.79 (m, 2H, H₁', H₃'), 6.87 (d, 1H, *J* = 8 Hz, H₄'), 7.30 (t, 1H, *J* = 7 Hz, H₃), 7.65 (d, 1H, *J* = 8 Hz, H₁), 7.81 (d, 2H, *J* = 8 Hz, H₁'', H₅''), 7.79 (d, 3H, *J* = 8 Hz, H₂'', H₄'', ArNH), 8.46 (s, 1H, N=CH), 8.97 (s, 1H, OH), 11.91 (s, 1H, O=CNH). ¹³C NMR (100 MHz, DMSO-*d*₆) δ (ppm; Figure S12): 45.05 (CH₂), 55.72 (C8), 112.09 (C₄'), 112.37 (C2), 113.90 (C6), 114.76 (C4), 114.60 (C₁'), 117.96 (C₃'), 125.22 (CF₃), 125.72 (C₁' and C₅''), 127.54 (C₂' and C₄''), 128.77

(C₁), 129.67 (C₃''), 131.59 (C3), 133.03 (C₂'), 138.49 (C₆''), 145.31 (C=N), 146.65 (C₆'), 146.75 (C5), 149.10 (C₅'). IR (ATR, cm⁻¹; Figure S22): 3,408, 3,221, 3,048, 1,638. ESI-MS (Figure S38): calculated for C₂₃H₂₀N₃O₃F₃: [M]⁺ = 443.14. Found: [M+H]⁺ = 444.09.

N'-(4-Nitrobenzylidene)-2-[[3-hydroxy-4-methoxybenzyl)amino]-benzohydrazide (**9g**)

Derivative **9g** was obtained by condensation of intermediate **13** with 1 equivalent of aldehyde **14g** (0.15 g, 1.0 mmol) in 40% yield. **9g** was purified by recrystallization with ethanol to give an orange solid; mp. 188–189°C; purity (HPLC; Figure S31): 98.9%. ¹H NMR (400 MHz, DMSO-*d*₆) δ (ppm; Figure S13): 3.73 (s, 3H, OCH₃), 4.25 (d, 2H, *J* = 5 Hz, CH₂), 6.63 (t, 1H, *J* = 7 Hz, 2H), 6.70 (d, 1H, *J* = 8 Hz, H₄), 6.74–6.80 (m, 2H, H₁', H₃'), 6.87 (d, 1H, *J* = 8 Hz, H₄'), 7.30 (t, 1H, *J* = 7 Hz, H₃), 7.66 (d, 1H, *J* = 8 Hz, H₁), 7.90 (s, 1H, ArNH), 7.97 (d, 2H, *J* = 9 Hz, H₂'', H₄''), 8.30 (d, 2H, *J* = 8 Hz, H₁'', H₅''), 8.49 (s, 1H, N=CH), 8.98 (s, 1H, OH), 12.01 (s, 1H, O=CNH). ¹³C NMR (100 MHz, DMSO-*d*₆) δ (ppm; Figure S14): 45.78 (CH₂), 55.72 (C8), 111.79 (C₄'), 112.41 (C2), 113.42 (C6), 114.39 (C4), 114.53 (C₁'), 117.87 (C₃'), 124.08 (C₁' and C₅''), 127.86 (C₂' and C₄''), 128.75 (C₁), 131.79 (C3), 133.16 (C₂'), 140.84 (C₃''), 144.45 (C=N), 146.63 (C₆'), 146.71 (C5), 147.77 (C₆''), 149.51 (C₅'). IR (ATR, cm⁻¹; Figure S23): 3,393, 3,229, 1,638, 1,520, 1,306. ESI-MS (Figure S39): calculated for C₂₂H₂₀N₄O₅: [M]⁺ = 420.14. Found: [M+H]⁺ = 421.04.

N'-(4-Cyanobenzylidene)-2-[[3-hydroxy-4-methoxybenzyl)amino]-benzohydrazide (**9h**)

Derivative **9h** was obtained by condensation of intermediate **13** with 1 equivalent of aldehyde **14h** (0.13 g, 1.0 mmol) in 43% yield. **9h** was purified by recrystallization with ethanol to give a light-green solid; mp. 191–192°C; purity (HPLC; Figure S32): 96.7%. ¹H NMR (400 MHz, DMSO-*d*₆) δ (ppm; Figure S15): 3.73 (s, 3H, OCH₃), 4.24 (d, 2H, *J* = 5 Hz, CH₂), 6.63 (t, 1H, *J* = 7 Hz, 2H), 6.70 (d, 1H, *J* = 8 Hz, H₄), 6.73–6.79 (m, 2H, H₁', H₃'), 6.87 (d, 1H, *J* = 8 Hz, H₄'), 7.29 (t, 1H, *J* = 7 Hz, H₃), 7.65 (dd, 1H, *J* = 8 Hz, 2 Hz, H₁), 7.89 (m, 5H, H₁'', H₂'', H₄'', H₅'', ArNH), 8.44 (s, 1H, N=CH), 8.95 (s, 1H, OH), 11.93 (s, 1H, O=CNH). ¹³C NMR (100 MHz, DMSO-*d*₆) δ (ppm; Figure S16): 45.82 (CH₂), 55.75 (C8), 111.17 (C₆''), 111.81 (C₄'), 112.44 (C2), 113.54 (C₆'), 114.44 (C4), 114.56 (C₁'), 117.93 (C₃'), 118.72 (C=N), 127.56 (C₂' and C₄''), 128.77 (C₁), 131.84 (C3), 132.78 (C₁' and C₅''), 133.15 (C₂'), 139.00 (C₆''), 145.05 (C=N), 146.05 (C₆'), 146.66 (C5), 149.51 (C₅'). IR (ATR, cm⁻¹; Figure S24): 3,378, 3,208, 3,031, 2,231, 1,638. ESI-MS (Figure S40): calculated for C₂₃H₂₀N₄O₃: [M]⁺ = 400.15. Found: [M+H]⁺ = 401.02.

4.2 | Pharmacological/biological assays

4.2.1 | VEGFR-2 inhibition assay

The enzymatic screening assay was performed by CEREP (France) with the TR-FRET LANCE phosphorylation methodology (www.cerep.fr) in 1 μM concentration. The standard used by CEREP was

staurosporine, which has an IC_{50} value of 3 nM for VEGFR-2. Inhibition percentages are calculated by the ratio of the percent inhibition of the compound to the percent inhibition of the standard (Figure S43). The assays are registered with the following study numbers: 100033826 (February 2017) and 100040512 (June 2017).

4.2.2 | Angiogenesis investigation using in vivo and in vitro models

CAM angiogenesis assay

Fertilized chicken eggs (*Gallus gallus domesticus*) were disinfected with 70% alcohol and incubated vertically (eggs were placed with the air chamber up) at 37.5°C in a humidified incubator, and windowed at Day 8. The silicone rubber orthodontic o-ring (Morelli Ortodontia; 1/4" Médio; REF: 60.08.112) was placed on the surface of the CAM. VEGF (0.6 ng/CAM), with or without the studied substances (1.0 µg/CAM), inside of the ring was added. Antiangiogenic AAL-993 (1.5 µg) was combined with VEGF and used as a positive control. The eggs were incubated for an additional 48 hr in the same experimental conditions.

The chicken embryos were euthanized by freezing (−20°C for 1 hr) and the CAMs were fixed in formalin for 30 min. Then, the CAMs were collected and color images were obtained using a stereomicroscope (Zeiss STEMI 305). The angiogenesis quantification was performed according to Mangir et al.^[75] Briefly, the color images were converted into black and white using Adobe Photoshop CS6. The magenta, blue, cyan, and green colors were reduced to −200% and yellow color to 0%; however, red color was increased to 300%. In the next step, an area inside the ring was selected and cropped (the same region area for all images) using Fiji software (version 2.2.2-rc-69/1.52n). The background was subtracted and vessels area was evidenced. The data are presented as percentage of pixels in the analyzed ± standard deviation from images of the different groups, VEGF ($n = 42$), VEGF plus AAL-993 ($n = 7$), VEGF plus tested compounds ($n = 7$).

HUVEC tube formation assay

The capillary-like tube formation assay was performed using BD Matrigel™ Matrix (BD Biosciences, Bedford, MA) and 96-well plates (50 µl/well). Endothelial cells (1.5×10^4 cells/well) suspended in 100 µl of RPMI medium supplemented with 1% of fetal calf serum were added to each well in the presence of the compounds **9e** and **9f** at 0.1 µM or vehicle (DMSO). The plates were incubated at 37°C for 18 hr, and then images were captured at ×10 magnification with a ProgRes C3 camera (Jenoptik, Germany) coupled to an inverted light microscope (Zeiss, Germany). The number of nodes, junctions, and meshes from three different wells was determined using Angiogenesis Analyzer from ImageJ Program. The data are presented as mean ± SD from two independent experiments performed in triplicate.

Statistical analysis

The statistical analysis was carried out with Jandel SigmaStat 3.1 software (Jandel Corporation, San Rafael, CA), using analysis of

variance, followed by post-hoc comparisons by the Holm–Sidak multiple comparison test or Dunnett's post-test.

4.3 | Molecular docking

In the molecular modeling study, a data collection of all the crystallographic structures available in the Protein Data Bank database (PDB; <http://www.rcsb.org>) for VEGFR-2 target proteins was carried out, followed by the analysis of their active site. The crystallographic structure of the VEGFR-2 enzyme with code 5EW358 and resolution 2.5 Å for docking was selected. Then, a molecular reanalysis (validation) was performed using the GOLD 5.2 program (CCDC; License: G/414/2006) with the four different punctuation functions available, that is, ASP, ChemPLP, ChemScore, and GoldScore. All of the aforementioned functions were evaluated by the reangling of the cocrystallized ligands to identify the punctuation function most appropriate to the study with the target protein. Validation of the docking run method using VEGFR-2 (5EW3) was performed with and without the water molecules of crystallization, spanning a set of amino acid residues within a 10 Å radius from the central amino acid Val899 to the ATP-binding site. After the re-anchoring step, root mean square deviation values between the best result of each scoring function and the crystallographic structure were calculated (Table S1). The ChemScore function showed the best performance (score: 0.3299; Figure S41). All the compounds were initially designed in Spartan'08 program (Wavefunction Inc.; DQAIR, USB-HASP) for the search of the lowest energy conformers using Hartree–Fock (calculation performed with base 3-21G) method. Docking runs were performed keeping the parameters defined in the validation step: the absence of water molecules, ChemScore function, and evaluation of a set of amino acid residues in a radius of 10 Å of distance from the central amino acid Val899 to the ATP-binding site. The conformation presenting the best mode of interaction and the best score value for each compound was analyzed separately. To evaluate the results, the PyMol program (License: 8588) was used, in which the graphical analyses of the obtained conformations and the numerical measures of the interatomic distances for the identified molecular interactions were obtained. Docking results of the compounds can be seen in Figures 3 and S42.

ACKNOWLEDGMENTS

The authors are grateful to Antonio M. Fregnan and Guilherme A. Ferreira-Silva for technical assistance in the cell viability assay. The authors are grateful for the financial support of Brazilian National Council of Research (CNPq Grant #465.249/2014-0, INCT-INOFAR).

CONFLICTS OF INTERESTS

The authors declare that there are no conflicts of interests.

ORCID

Eliezer J. Barreiro  <http://orcid.org/0000-0003-1759-0038>

REFERENCES

- [1] M. Rajabi, S. Mousa, *Biomedicines* **2017**, *5*, 34.
- [2] S. Qin, A. Li, M. Yi, S. Yu, M. Zhang, K. Wu, *J. Hematol. Oncol.* **2019**, *12*, 1.
- [3] L. M. Sherwood, E. E. Parris, J. Folkman, *N. Engl. J. Med.* **1971**, *258*, 1182.
- [4] P. Carmeliet, R. K. Jain, *Nature* **2000**, *407*, 249.
- [5] T. Tonini, F. Rossi, P. P. Claudio, *Oncogene* **2003**, *22*, 6549.
- [6] H. Fan, D. Wei, K. Zheng, X. Qin, L. Yang, Y. Yang, Y. Duan, Y. Xu, L. Hu, *Eur. J. Med. Chem.* **2019**, *175*, 349.
- [7] N. Nishida, H. Yano, T. Nishida, T. Kamura, M. Kojiro, *Vasc. Health Risk Manage.* **2006**, *2*, 213.
- [8] N. Ferrara, R. S. Kerbel, *Nature* **2005**, *438*, 967.
- [9] J. Folkman, *Semin. Oncol.* **2002**, *29*, 16.
- [10] D. Xu, T.-L. Wang, L.-P. Sun, Q.-D. You, *Mini-Rev. Med. Chem.* **2011**, *11*, 18.
- [11] G. K.ri, L. Trfi, G. N, meth, M. Hamacher, Wiley-VCH Verlag GmbH & Co. KGaA, Weinheim **2011**.
- [12] M. L. D. C. Barbosa, L. M. Lima, R. Tesch, C. M. Sant'Anna, F. Totzke, M. H. Kubbutat, C. Schächtele, S. A. Laufer, E. J. Barreiro, *Eur. J. Med. Chem.* **2014**, *71*, 1.
- [13] N. Ferrara, H. P. Gerber, J. LeCouter, *Nat. Med.* **2003**, *9*, 669.
- [14] G. Martiny-Baron, D. Marmé, *Curr. Opin. Biotechnol.* **1995**, *6*, 675.
- [15] A. Markowska, S. Sajdak, J. Markowska, A. Huczynski, *Eur. J. Med. Chem.* **2017**, *142*, 87.
- [16] C. S. Abhinand, R. Raju, S. J. Soumya, P. S. Arya, P. R. Sudhakaran, *J. Cell Commun. Signal.* **2016**, *10*, 347.
- [17] A. Chaikuad, P. Koch, S. A. Laufer, S. Knapp, *Angew. Chem., Int. Ed.* **2018**, *57*, 4372.
- [18] P. Koch, S. A. Laufer, *Molecules* **2018**, *23*, 5.
- [19] V. P. Chekhonin, S. A. Shein, A. A. Korchagina, O. I. Gurina, *Curr. Cancer Drug Targets* **2013**, *13*, 423.
- [20] S. Li, H.-X. Xu, C.-T. Wu, W.-Q. Wang, W. Jin, H.-L. Gao, H. Li, S.-R. Zhang, J.-Z. Xu, Z.-H. Qi, Q.-X. Ni, X.-J. Yu, L. Liu, *Angiogenesis* **2019**, *22*, 15.
- [21] M. A. Zeidan, A. S. Mostafa, R. M. Gomaa, L. A. Abou-zeid, M. El-Mesery, M. A.-A. El-Sayed, K. B. Selima, *Eur. J. Med. Chem.* **2019**, *168*, 315.
- [22] A. M. Al-Abd, A. J. Alamoudi, A. B. Abdel-Naim, T. A. Neamatallah, O. M. Ashour, *J. Adv. Res.* **2017**, *8*, 591.
- [23] L. S. Rosen, *Cancer Control* **2002**, *9*, 36.
- [24] H. L. Goel, A. M. Mercurio, *Nat. Rev. Cancer* **2013**, *13*, 871.
- [25] S. Yu, J. Oh, F. Li, Y. Kwon, H. Cho, J. Shin, S. K. Lee, S. Kim, *ACS Med. Chem. Lett.* **2017**, *8*, 1066.
- [26] J. Ma, D. J. Waxman, *Mol. Cancer Ther.* **2008**, *7*, 3670.
- [27] P. Wu, T. E. Nielsen, M. H. Clausen, *Trends Pharmacol. Sci.* **2015**, *36*, 422.
- [28] S. J. Modi, V. M. Kulkarni, *Med. Drug Discov.* **2019**, *2*, 100009.
- [29] R. Roskoski, *Pharmacol. Res.* **2019**, *144*, 19.
- [30] S. Wilhelm, C. Carter, M. Lynch, T. Lowinger, J. Dumas, R. A. Smith, B. Schwartz, R. Simantov, S. Kelley, *Nat. Rev. Drug Discov.* **2006**, *5*, 835.
- [31] R. C. Kane, A. T. Farrell, H. Saber, S. Tang, G. Williams, J. M. Jee, C. Liang, B. Booth, N. Chidambaram, D. Morse, R. Sridhara, P. Garvey, R. Justice, R. Pazdur, *Clin. Cancer Res.* **2006**, *12*, 7271.
- [32] D. B. Mendel, A. D. Laird, X. Xin, S. G. Louie, J. G. Christensen, G. Li, R. E. Schreck, T. J. Abrams, T. J. Ngai, L. B. Lee, L. J. Murray, J. Carver, E. Chan, K. G. Moss, J. Ö. Haznedar, J. Sukbuntherng, R. A. Blake, L. Sun, C. Tang, T. Miller, S. Shirazian, G. McMahon, J. M. Cherrington, *Clin. Cancer Res.* **2003**, *9*, 327.
- [33] R. J. Motzer, B. I. Rini, R. M. Bukowski, B. D. Curti, D. J. George, G. R. Hudes, B. G. Redman, K. A. Margolin, J. R. Merchan, G. Wilding, M. S. Ginsberg, J. Bacik, S. T. Kim, C. M. Baum, M. Dror Michaelson, *JAMA* **2006**, *295*, 2516.
- [34] H. Huynh, V. C. Ngo, S. P. Choo, D. Poon, H. N. Koong, C. H. Thng, H. C. Toh, L. Zheng, L. C. Ong, Y. Jin, I. C. Song, A. P. C. Chang, H. S. Ong, A. Y. F. Chung, P. K. H. Chow, K. C. Soo, *Curr. Cancer Drug Targets* **2009**, *9*, 738.
- [35] Y.-J. Bang, Y.-K. Kang, W. K. Kang, N. Boku, H. C. Chung, J.-S. Chen, T. Doi, Y. Sun, L. Shen, S. Qin, W.-T. Ng, J. M. Tursi, M. J. Lechuga, D. R. Lu, A. Ruiz-Garcia, A. Sobrero, *New Drugs* **2001**, *29*, 1449.
- [36] H. S. Rugo, R. S. Herbst, G. Liu, J. W. Park, M. S. Kies, H. M. Steinhardt, Y. K. Pithavala, S. D. Reich, J. L. Freddo, G. Wilding, *J. Clin. Oncol.* **2005**, *23*, 5474.
- [37] D. D. Hu-Lowe, H. Y. Zou, M. L. Grazzini, M. E. Hallin, G. R. Wickman, K. Amundson, J. H. Chen, D. A. Rewolinski, S. Yamazaki, E. Y. Wu, M. A. McTigue, B. W. Murray, R. S. Kania, P. O'Connor, D. R. Shalinsky, S. L. Bender, *Clin. Cancer Res.* **2008**, *14*, 7272.
- [38] Y. Zakharia, K. Zakharia, O. Rixe, *Drug Discov.* **2015**, *10*, 925.
- [39] F. M. Yakes, J. Chen, J. Tan, K. Yamaguchi, Y. Shi, P. Yu, F. Qian, F. Chu, F. Bentzien, B. Cancilla, J. Orf, A. You, A. D. Laird, S. Engst, L. Lee, J. Lesch, Y.-C. Chou, A. H. Joly, *Mol. Cancer Ther.* **2011**, *10*, 2298.
- [40] H. Singh, M. Brave, J. A. Beaver, J. Cheng, S. Tang, E. Zahalka, T. R. Palmbly, R. Venugopal, P. Song, Q. Liu, C. Liu, J. Yu, X. H. Chen, X. Wang, Y. Wang, P. G. Kluetz, S. R. Daniels, E. J. Papadopoulos, R. Sridhara, A. E. McKee, A. Ibrahim, G. Kim, R. Pazdur, *Clin. Cancer Res.* **2016**, *23*, 330.
- [41] B. Izar, W. Sharfman, F. S. Hodi, D. Lawrence, K. T. Flaherty, R. Amaravadi, K. B. Kim, I. Puzanov, J. Sosman, R. Dummer, S. M. Goldinger, L. Lam, S. Kakar, Z. Tang, O. Krieter, D. F. McDermott, M. B. Atkins, *Cancer Med.* **2017**, *6*, 1904.
- [42] D. Schiff, S. Kesari, J. de Groot, T. Mikkelsen, J. Drappatz, T. Coyle, L. Fichtel, B. Silver, I. Walters, D. Reardon, *Invest. New Drugs* **2015**, *33*, 247.
- [43] G. Bold, K.-H. Altmann, J. Frei, M. Lang, P. W. Manley, P. Traxler, B. Wietfeld, J. Brügggen, E. Buchdunger, R. Cozens, S. Ferrari, P. Furet, F. Hofmann, G. Martiny-Baron, J. Mestan, J. Rösel, M. Sills, D. Stover, F. Acemoglu, E. Boss, R. Emmenegger, L. Lässer, E. Masso, R. Roth, C. Schlachter, W. Vetterli, D. Wyss, J. M. Wood, *J. Med. Chem.* **2000**, *43*, 2310.
- [44] J. M. Wood, G. Bold, E. Buchdunger, R. Cozens, S. Ferrari, J. Frei, F. Hofmann, J. Mestan, H. Mett, T. O'Reilly, E. Persohn, J. Rösel, C. Schnell, D. Stover, A. Theuer, H. Towbin, F. Wenger, K. Woods-Cook, A. Menrad, G. Siemeister, M. Schirner, K.-H. Thierauch, M. R. Schneider, J. Dreves, G. Martiny-Baron, F. Totzke, D. Marmé, *Cancer Res.* **2000**, *60*, 2178.
- [45] H. Hess-Stunpp, M. Haberey, K. H. Thierauch, *ChemBioChem* **2005**, *6*, 550.
- [46] E. N. Scott, G. Meinhardt, C. Jacques, D. Laurent, A. L. Thomas, *Expert Opin. Invest. Drugs* **2007**, *16*, 367.
- [47] P. W. Manley, P. Furet, G. Bold, J. Brügggen, J. Mestan, T. Meyer, C. R. Schnell, J. Wood, M. Haberey, A. Huth, M. Krüger, A. Menrad, E. Ottow, D. Seidelmann, G. Siemeister, K.-H. Thierauch, *J. Med. Chem.* **2002**, *45*, 5687.
- [48] P. W. Manley, G. Bold, J. Brügggen, G. Fendrich, P. Furet, J. Mestan, C. Schnell, B. Stolz, T. Meyer, B. Meyhack, W. Stark, A. Strauss, J. Wood, *Biochim. Biophys. Acta, Proteins Proteomics* **2004**, *1697*, 17.
- [49] B. Kuhn, P. Mohr, M. Stahl, *J. Med. Chem.* **2010**, *53*, 2601.
- [50] A. Jansma, Q. Zhang, B. Li, Q. Ding, T. Uno, B. Bursulaya, Y. Liu, P. Furet, N. S. Gray, B. H. Geierstanger, *J. Med. Chem.* **2007**, *50*, 5875.
- [51] M. K. AbdElhameid, M. B. Labib, A. T. Negmeldin, M. Al-Shorbagy, M. R. Mohammed, *J. Enzyme Inhib. Med. Chem.* **2018**, *33*, 1472.
- [52] Y.-J. Wang, R. J. Kathawala, Y.-K. Zhang, A. Patel, P. Kumar, S. Shukla, K. L. Fung, S. V. Ambudkar, T. T. Talele, Z.-S. Chena, *Biochem. Pharmacol.* **2014**, *90*, 367.
- [53] A. Polverino, A. Coxon, C. Starnes, Z. Diaz, T. DeMelfi, L. Wang, J. Bready, J. Estrada, R. Cattley, S. Kaufman, D. Chen, Y. Gan, G. Kumar, J. Meyer, S. Neervannan, G. Alva, J. Talvenheimo, S. Montestruque, A. Tasker, V. Patel, R. Radinsky, R. Kendall, *Cancer Res.* **2006**, *66*, 8715.
- [54] J. L. Kim, D. A. Whittington, A. M. Long, P. Rose, Y. Gu, H. Zhao, *Protein Data Bank* **2008**, <https://doi.org/10.2210/pdb3EFL/pdb>

- [55] F. Petti, A. Thelemann, J. Kahler, S. McCormack, L. Castaldo, T. Hunt, L. Nuwaysir, L. Zeiske, H. Haack, L. Sullivan, A. Garton, J. D. Haley, *Mol. Cancer Ther.* **2005**, *4*, 1186.
- [56] A. J. Garton, A. P. A. Crew, M. Franklin, A. R. Cooke, G. M. Wynne, L. Castaldo, J. Kahler, S. L. Winski, A. Franks, E. N. Brown, M. A. Bittner, J. F. Keily, P. Briner, C. Hidden, M. C. Srebernak, C. Pirrit, M. O'Connor, A. Chan, B. Vulevic, D. Henninger, K. Hart, R. Sennello, A.-H. Li, T. Zhang, F. Richardson, D. L. Emerson, A. L. Castelhana, L. D. Arnold, N. W. Gibson, *Cancer Res.* **2006**, *66*, 1015.
- [57] T. A. Yap, H.-T. Arkenau, D. R. Camidge, S. George, N. J. Serkova, S. J. Gwyther, J. L. Spratlin, R. Lal, J. Spicer, N. M. Desouza, M. O. Leach, J. Chick, S. Poondru, R. Boinpally, R. Gedrich, K. Brock, A. Stephens, S. G. Eckhardt, S. B. Kaye, G. Demetri, M. Scurr, *Clin. Cancer Res.* **2013**, *19*, 909.
- [58] G. Bold, C. Schnell, P. Furet, P. McSheehy, J. Brügggen, J. Mestan, P. W. Manley, P. Drückes, M. Burglin, U. Dürler, J. Loretan, R. Reuter, M. Wartmann, A. Theuer, B. Bauer-Probst, G. Martiny-Baron, P. Allegrini, A. Goepfert, J. Wood, *J. Med. Chem.* **2016**, *59*, 132.
- [59] S. Thota, D. A. Rodrigues, P. de, S. M. Pinheiro, L. M. Lima, C. A. M. Fraga, E. J. Barreiro, *Bioorganic Med. Chem. Lett.* **2018**, *28*, 2797.
- [60] L. M. Lima, E. J. Barreiro, *Curr. Med. Chem.* **2005**, *12*, 23.
- [61] L. M. Lima, E. J. Barreiro, *Comprehensive Medicinal Chemistry III*, 3rd ed. (Eds: S. Chackalamannil, D. P. Rotella, S. E. Ward), Elsevier, Oxford **2017**, pp. 186–210.
- [62] E. J. Barreiro, C. A. M. Fraga, A. L. P. Miranda, C. R. Rodrigues, *Quim. Nova* **2002**, *25*, 129.
- [63] A.-G. El-Helby, R. R. A. Ayyad, H. Sakr, K. El-Adl, M. M. Ali, F. Khedr, *Arch. Pharm. Chem. Life Sci.* **2017**, *350*, e1700240.
- [64] H. T. Abdel-Mohsen, E. A. Abd El-Meguid, A. M. El Kerdawy, A. E. E. Mahmoud, M. M. Ali, *Arch. Pharm.* **2020**, *353*, e1900340.
- [65] R. F. Borch, M. D. Bernstein, H. D. Durst, *J. Am. Chem. Soc.* **1971**, *93*, 2897.
- [66] T. F. Gomes, T. E. T. Pompeu, D. A. Rodrigues, F. Noël, R. Menegattia, C. H. Andrade, J. R. Sabino, E. S. Gila, T. D. Costa, A. H. Betti, C. B. Antonio, S. M. K. Rates, C. A. M. Fraga, E. J. Barreiro, V. de Oliveira, *Eur. J. Med. Chem.* **2013**, *62*, 214.
- [67] A. E. Kümmerle, M. Schmitt, S. V. S. Cardozo, C. Lugnier, P. Villa, A. B. Lopes, N. C. Romeiro, H. Justiniano, M. A. Martins, C. A. M. Fraga, J.-J. Bourguignon, E. J. Barreiro, *J. Med. Chem.* **2012**, *55*, 7525.
- [68] C. A. M. Fraga, E. J. Barreiro, *Curr. Med. Chem.* **2006**, *13*, 167.
- [69] E. I. Deryugina, J. P. Quigley, *Methods Enzymol.* **2008**, *444*, 21.
- [70] X. Yuan, Q. Yangaf, T. Liu, K. Li, Y. Liu, C. Zhu, Z. Zhang, L. Li, C. Zhang, M. Xie, J. Lin, J. Zhang, Y. Jin, *Eur. J. Med. Chem.* **2019**, *179*, 147.
- [71] H. T. Abdel-Mohsen, A. S. Girgis, A. E. E. Mahmoud, M. M. Ali, D. I. El Diwani, *Arch. Pharm. Chem. Life Sci.* **2019**, *352*, e1900089.
- [72] G. Shen, Y. Li, T. Du, G. Shi, L. Dai, X. Chen, R. Zheng, W. Li, X. Su, S. Zhang, Y. Wei, S. Yang, H. Deng, *Neoplasma* **2012**, *59*, 486.
- [73] N. S. Vasudev, A. R. Reynolds, *Angiogenesis* **2014**, *17*, 471.
- [74] R. Ronca, M. Benkheil, S. Mitola, S. Struyf, S. Liekens, *Med. Res. Rev.* **2017**, *37*, 1231.
- [75] N. Mangir, A. Raza, J. W. Haycock, C. Chapple, S. Macneil, *In Vivo* **2018**, *32*, 461.

SUPPORTING INFORMATION

Additional supporting information may be found online in the Supporting Information section.

How to cite this article: Pauli FP, Martins JR, Paschoalin T, Ionta M, Barbosa MLC, Barreiro EJ. Novel VEGFR-2 inhibitors with an *N*-acylhydrazone scaffold. *Arch Pharm.* 2020;e2000130. <https://doi.org/10.1002/ardp.202000130>